PHYSICAL REVIEW E **89**, 041004(R) (2014)

Strong pinning of propagation fronts in adverse flow

Thomas Gueudré,[1,*] Awadhesh Kumar Dubey,[2] Laurent Talon,[2] and Alberto Rosso[3]
[1]*CNRS-LPT, Ecole Normale Supérieure, 75231 Cedex 05 Paris, France*
[2]*Université Paris-Sud, CNRS, Laboratoire FAST, UMR 7608, Orsay F-91405, France*
[3]*Université Paris-Sud, CNRS, LPTMS, UMR 8626, Orsay F-91405, France*
(Received 14 February 2014; published 18 April 2014)

Reaction fronts evolving in a porous medium exhibit a rich dynamical behavior. In the presence of an adverse flow, experiments show that the front slows down and eventually gets pinned, displaying a particular sawtooth shape. Extensive numerical simulations of the hydrodynamic equations confirm the experimental observations. Here we propose a stylized model, predicting two possible outcomes of the experiments for large adverse flow: either the front develops a sawtooth shape or it acquires a complicated structure with islands and overhangs. A simple criterion allows one to distinguish between the two scenarios and its validity is reproduced by direct hydrodynamical simulations. Our model gives a better understanding of the transition and is relevant in a variety of domains, when the pinning regime is strong and only relies on a small number of sites.

DOI: 10.1103/PhysRevE.89.041004 PACS number(s): 47.54.−r, 82.33.Ln

In the systems separated in distinct phases, the dynamics is controlled by the behavior of the propagating fronts. Those fronts pervade a broad variety of domains in physics, ranging from chemotaxis [1] and plasma physics [2] to flame fronts [3] or epidemics, therefore triggering much activity in their modeling (for a recent review, see [4]). One of the cornerstones in this field is the celebrated Fisher–Kolmogorov-Petrowsky-Piscunov (FKPP) theory, describing the front propagation in reaction-diffusion systems [5]. However, this approach was limited to systems with no advection, i.e., not undergoing any fluid flow, despite its physical importance. Coherent fluidlike motion strongly impacts the dynamics of the fronts [6] and remains a challenging problem, whether because of the appearance of turbulence [7] or because of the influence of a disordered media [8,9]. One natural disordered environment for propagation fronts is a porous medium. Some examples were investigated in the petroleum industry and aeronautics with attempts to address the evolution of a flame front in a gas filter [10,11]. Recently, experiments on self-sustained chemical reactions have allowed a fine and controlled examination of the propagation fronts in a porous medium, revealing some striking features by direct observation [12].

The experimental setup employs an autocatalytic reaction invading a cell filled with a solution of reactants. To reproduce porosity, the cell also contains a mixture of glass spheres of different sizes. The reaction starts at the bottom of the cell and, in the absence of advection flow, develops into an almost flat front propagating upwards with constant chemical speed $|V_\chi| = \sqrt{D_m \alpha/2}$ and width $\ell_\chi = D_m/|V_\chi|$, with D_m being the molecular diffusion constant and α the reaction rate. In the presence of an adverse flow injected from the top at speed $\overline{U}$, the porosity generates a fixed random velocity map of the fluid with short range correlations of characteristic length ℓ_d. A rich dynamical phase diagram is observed as a function of the flow velocity $\overline{U}$, which is the control parameter of the experiment (see Fig. 1). In particular, the self-sustained fronts can travel downstream along the flow (D), remain static over a range of flow rate values (S), or move upstream (Up). In all of these phases, the heterogeneities make the front rough and the dynamics proceeds by random jumps called avalanches displaying a free scale statistics.

Here we focus on the transition between the static and the downstream regimes, occurring at the threshold U_{SD} (see Fig. 1). Hydrodynamical simulations show two different scenarios: either the invading chemical reaction is completely washed away for $\overline{U} > U_{SD}$ or some stagnant chemicals remain trapped in the porous media for any $\overline{U}$. In the first case, approaching U_{SD} from below, the front is largely deformed into a sawteeth structure (see Fig. 1, bottom right), while in the second case, the interface adopts a very rough and complicated structure with overhangs (see Fig. 1, bottom left). Experiments typically correspond to the first scenario but the second one has also been observed in very contaminated cells [12].

In this Rapid Communication, we describe the front propagation with a stylized model controlled by two parameters that can be easily measured in experiments. This model gives a simple criterion to discriminate between both scenarios, depending only on the behavior of the disorder distribution close to 0. The critical threshold U_{SD} and the shape of the front can be characterized. Comparison with hydrodynamical *ab initio* simulations using the Darcy equation shows a perfect agreement with our results. Although our approach addresses questions raised by the experiments of [12], the results of this stylized model are much more general and relevant to all systems where the transition between a static and a moving regime is controlled by a small number of pinning sites [13–16].

From first-principles hydrodynamics to a simple statistical model. The flow field $\vec{U}(\vec{r})$ can be computed via the Darcy-Brinkman equation:

$$\vec{\nabla} \cdot \vec{U}(\vec{r}) = 0, \tag{1}$$

$$\vec{U}(\vec{r}) = -\frac{K(\vec{r})}{\eta}\vec{\nabla} P + K(\vec{r})\Delta\vec{U}, \tag{2}$$

where $P(\vec{r})$ is the pressure field, η is the fluid viscosity, and $K(\vec{r})$ is the local permeability. Due to the incompressibility,

*thomas.gueudre@lpt.ens.fr

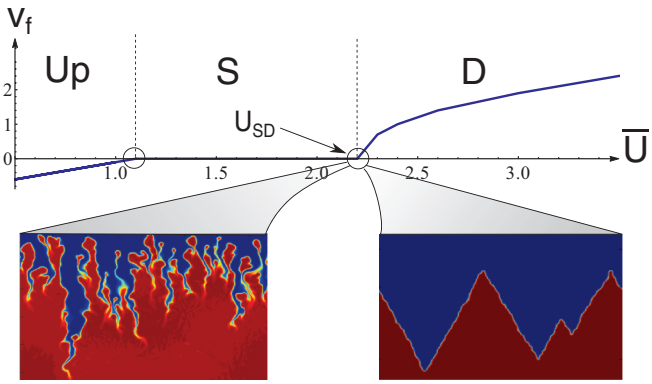

FIG. 1. (Color online) Average speed of the front V_f as a function of the injection speed $\overline{U}$ (the convention chosen is $\overline{U} > 0$ for a flow from top to bottom of the cell). Depending on the sign of V_f, the different regimes Up, S, and D are defined. For $\overline{U} = U_{SD}$, we observe a transition between a static front ($V_f = 0$) and a downstream front ($V_f > 0$). Bottom part: Hydrodynamical simulations of the front, for $\overline{U} \sim U_{SD}$ and for different permeability distributions. Two scenarios are observed: a regular sawtooth shape (right) or a complicated shape with overhangs (left).

the mean fluid velocity is fixed to the injection rate $\overline{U}$. Once the hydrodynamic problem is solved, the concentration of the chemicals $C(\vec{r},t)$ obeys an advection-diffusion equation (see [17]):

$$\frac{\partial C}{\partial t} + \vec{U} \cdot \vec{\nabla} C = D_m \Delta C + \alpha C^2 (1 - C). \tag{3}$$

The effect of the disorder is incorporated in the permeability $K(\vec{r})$, usually modeled as a random field, correlated over a distance ℓ_d. Here we study the front geometry for different permeability distributions: the log-normal distribution, often employed to model permeability [18], and the distributions belonging to the Weibull family of parameter δ. Figure 1 displays typical fronts for both log-normal distributed (bottom left) and Weibull distributed (bottom right, with $\delta = 0.8$) permeability fields. Those are generated using a standard method detailed in the Supplemental Material [19]. Both $U(\vec{r})$ and $C(\vec{r},t)$ were solved using a lattice Boltzmann scheme (see [20,21]). We ran the simulations on a square grid of size $L = 512$, up to $N = 2000$ realizations.

In the experimental conditions $\ell_d \gg \ell_\chi$, the front lays in the so-called *thin front eikonal* limit [22,23]. In this limit, at each point of the front, the normal component of the interface velocity satisfies $\vec{V}_f(\vec{r}) \cdot \vec{n} = V_\chi + \vec{U}(\vec{r}) \cdot \vec{n} + D_m \kappa$, where $\vec{n}$ is the unit normal vector and κ is the curvature of the front. For $\overline{U} \sim U_{SD}$, $\vec{U}(\vec{r})$ is mainly directed along the y axis, $\vec{U}(\vec{r}) \sim [0, U(\vec{r})]$. It is natural to assume that $U(\vec{r})$ is constant on patches of area ℓ_d^2 and decorrelated between patches. The velocity of each patch is an independent random variable of average $\overline{U}$, distributed as

$$P_{\overline{U}}(U) = \frac{1}{\overline{U}} \phi(U/\overline{U}), \tag{4}$$

where the scaling function $\phi(v)$ is independent of $\overline{U}$. When $\overline{U} \leqslant U_{SD}$, the front is pinned by the very few stagnant sites where $U(\vec{r}) < |V_\chi|$. Hence the distance ℓ_Δ between

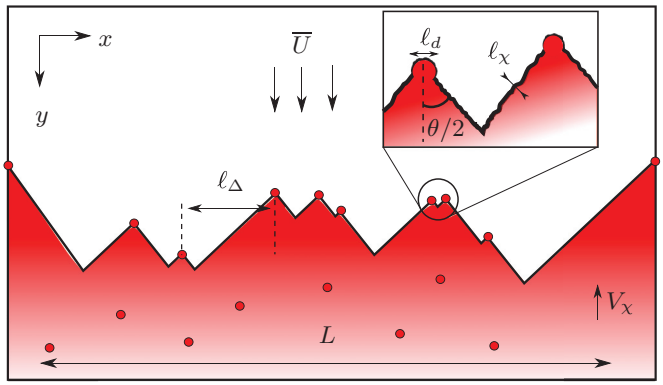

FIG. 2. (Color online) Sketch of the stylized model: in the thin eikonal limit $\ell_d \gg \ell_\chi$, the system can be described as a propagating front. Close to U_{SD}, the density of stagnant regions becomes small and the interface adopts a *sawtooth* structure.

them is much larger than ℓ_d. In the neighborhood of a pinning site, the front has a *sawtooth* shape of angle θ and the front displays a sawtoothlike structure (see Fig. 2). θ can be computed observing that, in that regime, $\kappa \simeq 0$, $V_f(\vec{r}) = 0$, and $U(\vec{r}) \simeq \overline{U}$, and thus the eikonal equation becomes [12]

$$V_\chi + \overline{U} \sin(\theta/2) = 0. \tag{5}$$

Therefore, the geometry of the frozen fronts is completely determined by the velocity-dependent angle θ and by the positions of the pinning sites. In particular, the probability that a given patch of area ℓ_d^2 is a pinning site is

$$\lambda = \int_0^{|V_\chi|} P_{\overline{U}}(U) dU = \int_0^{|V_\chi|/\overline{U}} \phi(v) dv. \tag{6}$$

For large downstream injection rate $\overline{U} \gg |V_\chi|$, the value of λ is controlled only by the behavior of $\phi(v)$ for v close to 0. In [12], it was observed that the fluid velocity vanishes near the wall. To mimic that fact, we always set the interface pinned at the points $\vec{r} = (0,0)$ and $\vec{r} = (L,0)$. Therefore, if no stagnant patch inside the cell pins the front, except at the walls, the interface acquires a V shape that we call the *depinned state*.

A central quantity for our analysis is $Q(y)$, i.e., the probability that, from $y = 0$ to y, no stagnant patch is encountered. $Q(y)$ obeys the differential equation,

$$Q(y + dy) = \left\{1 - \lambda dy [L - 2\tan(\theta/2) y]/\ell_d^2\right\} Q(y), \tag{7}$$

because the probability that no pinning occurs between y and $y + dy$ is $1 - \lambda dy[L - 2\tan(\theta/2)y]/\ell_d^2$ in an interval of size $L - 2\tan(\theta/2)\, y$. Hence,

$$Q(y) = e^{-\lambda [Ly - \tan(\theta/2) y^2]/\ell_d^2}. \tag{8}$$

This formula is valid up to $y_V = \frac{L}{2\tan(\theta/2)}$, the value above which the front is in the depinned state. This quantity allows one to introduce an efficient algorithm to generate the sites pinning the front: Note ϵ as a random number uniformly distributed in (0,1). If $\epsilon < Q(y_V)$, the algorithm terminates with a V shape, while if $\epsilon > Q(y_V)$, the height of the first pinning site is $y_1 = Q^{-1}(\epsilon)$ and its position x_1 is chosen at

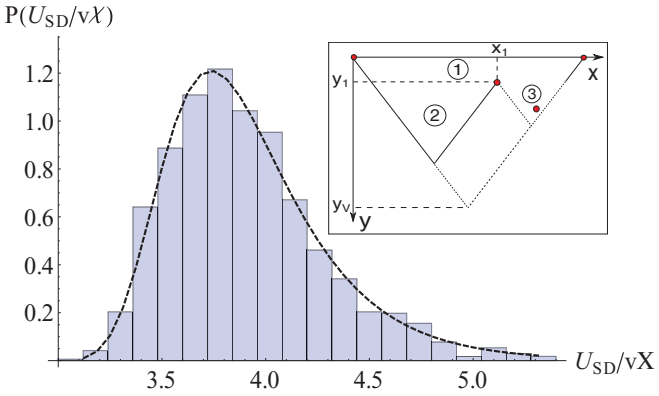

FIG. 3. (Color online) Probability distribution of the velocity threshold U_{SD}. The histogram corresponds to the hydrodynamical simulations of $N = 2000$ samples with a log-normal permeability, setting $L = 512$, $V_\chi = 0.0016$, $\overline{U} = 0.0036$, and $\ell_d = 5.0$. The dashed line corresponds to the prediction of the stylized model [Eq. (9)] for a log normal $\phi(v)$ with a scale parameter $\sigma = 0.315$ (see main text). Inset: Sketch of the algorithmic recursive procedure.

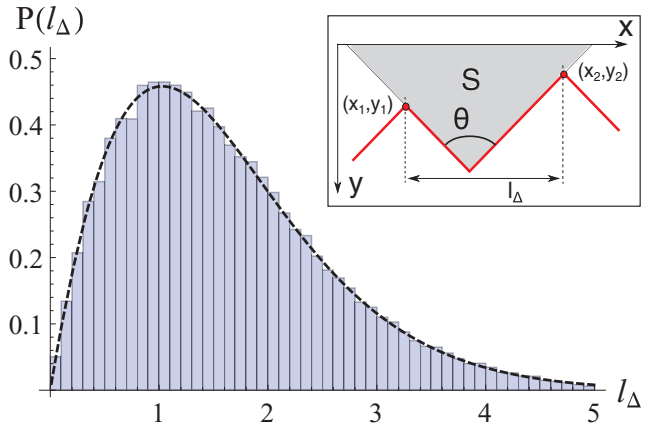

FIG. 4. (Color online) Distribution of l_Δ for the stylized model with parameters $\lambda = 0.5$ and $\theta = \pi/2$. The system size is $L = 100$ and the simulation is performed over $N = 3000$ samples. The dashed line corresponds to the asymptotic prediction of Eq. (15). Inset: Interface pinned between two adjacent stagnant patches of coordinates $\mathbf{x_1}$ and $\mathbf{x_2}$.

random in the segment of length $L - 2\tan(\theta/2)y_1$. This patch divides the segment into two pieces (see inset of Fig. 3) and we recursively apply the algorithm to both pieces until no more stagnant patch is found.

Moreover, Eq. (8) determines the statistics of the threshold U_{SD}. The probability of being in the depinned state for a certain injection rate $\overline{U}$ ($y = y_V$) is given by

$$Q_{\overline{U}}^{\rm dep} = \exp\left\{-\frac{L^2\int_0^{|V_\chi|/\overline{U}}\phi(v)dv}{\ell_d^2\tan[\arcsin(|V_\chi|/\overline{U})]}\right\}. \qquad (9)$$

We note that this probability goes to 0 quadratically in L. More generally, in d dimensions, $Q(y_V)$ would decay as $\exp(-L^{-d})$. Hence the effect of the cell size on the transition is very strong and explains why washing a propagating front in disordered medium can be surprisingly hard. With raising $\overline{U}$, Eq. (9) exhibits two competing effects: the stagnant patches get decimated, while the reaction front stretches (namely, $\theta \to 0$) and explores a larger region. Assuming $\phi(v) \sim v^{\delta-1}$ when $v \to 0$, we get

$$Q_{\overline{U}}^{\rm dep} = \exp\left[-\frac{L^2}{\ell_d^2}\left(\frac{|V_\chi|}{\overline{U}}\right)^{\delta-1}\right] \quad \text{when} \quad \frac{|V_\chi|}{\overline{U}} \to 0. \qquad (10)$$

The two scenarios pictured in Fig. 1 now emerge naturally: if $\delta > 1$, the number of teeth decreases with $\overline{U}$ and the interface always gets depinned, while if $\delta < 1$, the pinning sites proliferate and the front becomes rougher and rougher. As the formation of overhangs is expected, the stylized model breaks down. The transition between the two regimes occurs at a critical value $\delta_c = 1$: in that marginal case, the number of teeth remains constant. This prediction is well supported by the hydrodynamical simulations of the porous media for different $P_{\overline{U}}(v)$, where a clear transition towards roughening for $\delta < 1$ is observed. In the experiments, the measured velocity map was fitted to a log-normal distribution, decaying to 0 as $v^{-1}\exp[-\ln(v)^2]$, which is faster than the critical case, but not much. Hence, depinning indeed occurs. Note that the threshold speed U_{SD} is itself random and depends on the realization of the disorder. Its probability distribution $P(U_{SD}) = \partial_{\overline{U}} Q_{\overline{U}}^{\rm dep}|_{\overline{U}=U_{SD}}$ depends on the scaled velocity distribution $\phi(v)$. In Fig. 3, we test the prediction of our model against hydrodynamical simulations for a log-normal permeability. We assume that the velocity of the fluid displays as well a log-normal distribution, $\phi(v) = (\sqrt{2\pi}v\sigma)^{-1}e^{-(\ln v)^2/2\sigma^2}$, with a scale parameter $\sigma = 0.315$ obtained from the direct fit of the velocity distribution close to zero. A very good agreement *with no adjusting parameter* is observed.

To get a better grasp on the front roughness for $\overline{U} \lesssim U_{SD}$, we compute the distance l_Δ between two adjacent pinning sites. A scaling argument (that can be easily extended to various geometries) extracts the main dependence in λ and θ of the typical distance between stagnant patches: Let us assume the interface pinned at some site and consider its right part (see inset of Fig. 4). The probability of having another pinning is important when the area $S \sim l_\Delta^2/\tan(\theta/2) \sim \lambda^{-1}$, leading to

$$l_\Delta \sim \sqrt{\frac{\tan\theta/2}{\lambda}} = \ell_{\rm typ}. \qquad (11)$$

It turns out that it is possible to compute the whole probability distribution $\rho(l_\Delta)$ in the *sawtooth* geometry. It obeys

$$\rho(l_\Delta) = \int_{\mathcal{D}} d\mathbf{x}_1 d\mathbf{x}_2 P(\mathbf{x}_{12})\delta(l_\Delta - |x_2 - x_1|),$$
$$\mathcal{D} = \left\{0 < x_i < L, 0 < y_i < \min\left(\frac{x_i}{\tan\theta/2}, \frac{L - x_i}{\tan\theta/2}\right)\right\}, \qquad (12)$$

with $i \in \{1,2\}$. $\mathcal{D}$ simply parametrizes the area of the interface in the depinned state. $P(\mathbf{x}_{12})$ is the probability that the interface

is pinned in $\mathbf{x}_1 = (x_1, y_1)$ and $\mathbf{x}_2 = (x_2, y_2)$, with no other nucleation in between:

$$P(\mathbf{x}_{12})d\mathbf{x}_1 d\mathbf{x}_2 = \lambda^2 d\mathbf{x}_1 d\mathbf{x}_2 e^{-\lambda S(x_1,x_2,y_1,y_2)},$$
$$S(x_1,x_2,y_1,y_2) = \frac{\tan(\theta/2)}{4}\left[y_1 + y_2 + \frac{x_2 - x_1}{\tan(\theta/2)}\right]^2 \times H\left(|x_2 - x_1|/\tan(\theta/2) - |y_2 - y_1|\right), \tag{13}$$

with S being the triangular area depicted in the inset of Fig. 4 and H a Heaviside function. Integration over the variables under the constraint that $l_\Delta = |x_2 - x_1|$ leads, in the limit $L \to \infty$, to

$$\rho(l_\Delta) = \frac{1}{\ell_{\text{typ}}}\hat{\rho}(r) \quad \text{with } r = l_\Delta/\ell_{\text{typ}}, \tag{14}$$

$$\hat{\rho}(r) = \frac{2}{\sqrt{\pi}}\left\{2(e^{-\frac{r^2}{4}} - e^{-r^2}) + \sqrt{\pi}r\left[\text{erf}\left(\frac{r}{2}\right) - 2\text{erf}(r) + 1\right]\right\}. \tag{15}$$

The maximum of $\hat{\rho}$ is of the order of 1, recovering the scaling argument given in Eq. (11), and an excellent agreement with the stylized model is observed (see Fig. 4). This distribution gives full information about the fluctuations of the static front in the porous media and allows one, for example, to compute its lateral extension through $\overline{\Delta H} \sim l_\Delta/[2\tan(\theta/2)]$. Finer details about the statistical properties of the interface can be useful, for example, to study fluctuations of the critical currents of a strongly pinned vortex in superconductors [15].

In this Rapid Communication, we presented a general model of pinning for interfaces in random media, when the pinning regime is strong and only relies on a finite number of sites. This, in particular, makes an approach through Poisson processes possible, allowing at the same time efficient numerical simulations and analytical results on the statistical properties of the interface. The essential experimental picture [12] is reproduced and we identified a clear criterium that allows one to discriminate between the possible scenarios shown in Fig. 1. Supported by excellent agreement with *ab initio* simulations used to model the experiments [24], this validates the hypothesis that the depinning transition is controlled by a limited number of events, randomly spread over the medium.

The above model assumes that the interface is in its final state. However, strong pinning phenomena often exhibit avalanches during transient phases, where some stagnant patches temporarily pin the interface before getting suddenly depleted. The temporal critical properties of those systems are not well understood. As a perspective, it would hence be interesting to extend the present work to transient states by introducing the random lifetime of the nucleation events.

We gratefully acknowledge Severine Atis, Pierre Le Doussal, and Dominique Salin for useful discussions.

[1] J. Adler, Science **153**, 708 (1966).
[2] T. J. M. Boyd and J. J. Sanderson, *The Physics of Plasmas* (Cambridge University Press, Cambridge, 2003).
[3] J. Jarosinski and B. Veyssiere, *Combustion Phenomena: Selected Mechanisms of Flame Formation, Propagation and Extinction* (CRC, Boca Raton, FL, 2009).
[4] J. Fort and T. Pujol, Rep. Prog. Phys. **71**, 086001 (2008).
[5] R. A. Fisher, Ann. Eugenics **7**, 355 (1937).
[6] B. F. Edwards, Phys. Rev. Lett. **89**, 104501 (2002).
[7] M. E. Schwartz and T. H. Solomon, Phys. Rev. Lett. **100**, 028302 (2008).
[8] J. Xin, SIAM Rev. **42**, 161 (2000).
[9] I. V. Koptyug, V. Zhivonitko, and R. Sagdeev, J. Phys. Chem. B **112**, 1170 (2008).
[10] A. A. Korzhavin and V. A. Bunev, Combust. Flame **109**, 507 (1997).
[11] K. K. Kuo, R. Vichnevetsky, and M. Summerfield, AIAA J. **11**, 444 (1973).
[12] S. Atis, S. Saha, H. Auradou, D. Salin, and L. Talon, Phys. Rev. Lett. **110**, 148301 (2013).
[13] P. Yang and C. M. Lieber, J. Mater. Res. **12**, 2981 (1997).
[14] B. Maiorov, S. A. Baily, H. Zhou, O. Ugurlu, J. A. Kennison, P. C. Dowden, T. G. Holesinger, S. R. Foltyn, and L. Civale, Nat. Mater. **8**, 398 (2009).
[15] A. E. Koshelev and A. B. Kolton, Phys. Rev. B **84**, 104528 (2011).
[16] D. Dalmas, E. Barthel, and D. Vandembroucq, J. Mech. Phys. Solids **57**, 446 (2009).
[17] N. Jarrige, I. Bou Malham, J. Martin, N. Rakotomalala, D. Salin, and L. Talon, Phys. Rev. E **81**, 066311 (2010).
[18] G. Matheron, *Éléments Pour une Théorie des Milieux Poreux* (Masson et Cie, Paris, 1967).
[19] See Supplemental Material at http://link.aps.org/supplemental/10.1103/PhysRevE.89.041004 for the procedures to generate correlated Gaussian random fields.
[20] L. Talon, J. Martin, N. Rakotomalala, D. Salin, and Y. C. Yortsos, Water Resour. Res. **39**, 1135 (2003).
[21] I. Ginzburg, Phys. Rev. E **77**, 066704 (2008).
[22] M. Leconte, J. Martin, N. Rakotomalala, and D. Salin, Phys. Rev. Lett. **90**, 128302 (2003).
[23] F. Williams, *Combustion Theory*, 2nd ed. (Benjamin/Cummings, New York, 1985).
[24] S. Saha, S. Atis, D. Salin, and L. Talon, Europhys. Lett. **101**, 38003 (2013).